Elsevier Editorial System(tm) for International Journal of Multiphase Flow
Manuscript Draft

Manuscript Number:

Title: Gas-phase velocity fluctuations in statistically homogeneous fixed particle assemblies from particle-resolved direct numerical simulation

Article Type: Original Research Paper

Keywords: Gas-solid flow, Gas-phase velocity fluctuations, particle-resolved direct numerical simulation, immersed boundary method

Corresponding Author: Prof. Shankar Subramaniam, Ph.D.

Corresponding Author's Institution:

First Author: Sudheer Tenneti

Order of Authors: Sudheer Tenneti; Rahul Garg; Shankar Subramaniam, Ph.D.

Abstract: Gas-phase velocity fluctuations are quantified using particle-resolved direct numerical simulation (PR-DNS). The kinetic energy associated with the gas-phase velocity fluctuations k in steady flow past fixed random assemblies of monodisperse spheres is characterized as a function of solid volume fraction φ and the Reynolds number based on the mean slip velocity Re. The PR-DNS approach is based on a formulation we refer to as the Particle-resolved Uncontaminated-fluid Reconcilable Immersed Boundary Method (PUReIBM). A simple scaling analysis is used to explain the dependence of k on φ and Re. The steady value of k results from the balance between the source of k_ due to interphase transfer of kinetic energy, and the dissipation rate (ε) of k in the gas-phase. It is found that it is appropriate to model the dissipation rate of k in gas-solid flows using a length scale that is analogous to the Taylor microscale used in single-phase turbulence. Using the PUReIBM PR-DNS data for k and ε we also infer an eddy viscosity for gas-solid flow.

Cover Letter

095E, H. M. Black Engineering Building
Department of Mechanical Engineering
Iowa State University
Ames, IA 50011
Ph: (515) 294–0369
Fax: (515) 294–3261
email: sudheert@iastate.edu

April 10, 2012

Editorial Office,
International Journal of Multiphase Flow
Department of Mechanical Engineering
The John Hopkins University
Baltimore, MD 21218

Dear Sir/Madam:

Please find enclosed the manuscript of a paper that we would like to submit to *International Journal of Multiphase Flow* (IJMF) as a full–length article. The details of the manuscript are:

Title: "Gas–phase velocity fluctuations in statistically homogeneous fixed particle assemblies from particle–resolved direct numerical simulation"

Author: S. Tenneti, R. Garg, and S. Subramaniam

Journal: *International Journal of Multiphase Flow*

This paper is closely related to another article that we are simultaneously submitting to IJMF. The title of the second article is "Gas–phase velocity fluctuations in statistically homogeneous fixed particle beds and freely evolving suspensions using particle–resolved direct numerical simulation" and is authored by M. Mehrabadi, S. Tenneti, and S. Subramaniam. We bring this to your attention so that it may be factored into your review process.

PACS codes: 47.61.Jd, 47.55.Kf

This is previously unpublished work and has not been simultaneously submitted for publication elsewhere. Thank you.

Sincerely,

Sudheer Tenneti

Enclosures: One(1) copy of the manuscript

Highlights of "Gas–phase velocity fluctuations in statistically homogeneous fixed particle assemblies from particle–resolved direct numerical simulation"

- Level of gas–phase velocity fluctuations in gas–solid flow is quantified using particle-resolved simulation of flow past fixed spheres
- A Taylor microscale type length scale is found to be appropriate to model dissipation rate in gas–solid flows
- A new eddy viscosity model for gas–solid flows is proposed that can be used in CFD simulations of fluidized beds

Gas–phase velocity fluctuations in statistically homogeneous fixed particle assemblies from particle–resolved direct numerical simulation

S. Tenneti[a], R. Garg[a], S. Subramaniam[a,*]

[a]*Department of Mechanical Engineering, Center for Computational Thermal–fluids Research, Iowa State University,Ames, IA 50011, USA*

Abstract

Gas–phase velocity fluctuations are quantified using particle–resolved direct numerical simulation (PR–DNS). The kinetic energy associated with the gas–phase velocity fluctuations k_f in steady flow past fixed random assemblies of monodisperse spheres is characterized as a function of solid volume fraction ϕ and the Reynolds number based on the mean slip velocity Re_m. The PR–DNS approach is based on a formulation we refer to as the Particle–resolved Uncontaminated–fluid Reconcilable Immersed Boundary Method (PUReIBM). A simple scaling analysis is used to explain the dependence of k_f on ϕ and Re_m. The steady value of k_f results from the balance between the source of k_f due to interphase transfer of kinetic energy, and the dissipation (ε_f) of k_f in the gas–phase. It is found that it is appropriate to model the dissipation of k_f in gas–solid flows using a length scale that is analogous to the Taylor microscale used in single–phase turbulence. Using the PUReIBM PR–DNS data for k_f and ε_f we also infer an eddy viscosity

*Corresponding author
Email address: shankar@iastate.edu (S. Subramaniam)

for gas–solid flow.

1. Introduction

Gas-solid flows are encountered in industrial devices such as fluidized beds and in pneumatic conveying. It is generally agreed that gas–phase velocity fluctuations and particle–particle interactions play an important role in such gas–solid flows. For instance, the gas–solid flow in circulating fluidized bed risers is characterized by the tendency of the particles to segregate towards the pipe wall (Miller and Gidaspow, 1992). This can in turn affect the particle–wall heat transfer. Gas–phase velocity fluctuations also affect the heat transfer and mixing of chemical species inside the fluidized bed. Therefore, quantifying the level of gas–phase velocity fluctuations in canonical gas–solid flows is an important step towards understanding gas–solid flow in industrial devices.

Device–scale calculations using computational fluid dynamics (CFD) simulations of multiphase flow are a promising route to inexpensive design and scale–up of industrial process equipment (Halvorsen et al., 2003; Kashiwa and Gaffney, 2003; Sun et al., 2007). CFD of multiphase flow involves solving the averaged equations for mass, momentum and energy in both the solid and fluid phases. Figure 1 shows a schematic of the computational domain in a typical CFD simulation of gas–solid flow. In every grid cell, conservations equations for averaged quantities such as volume fraction, and velocity are solved for both phases. These conservation equations are obtained using a statistical averaging procedure (Anderson and Jackson, 1967; Drew and Passman, 1998), and hence the solution to these average equations involves

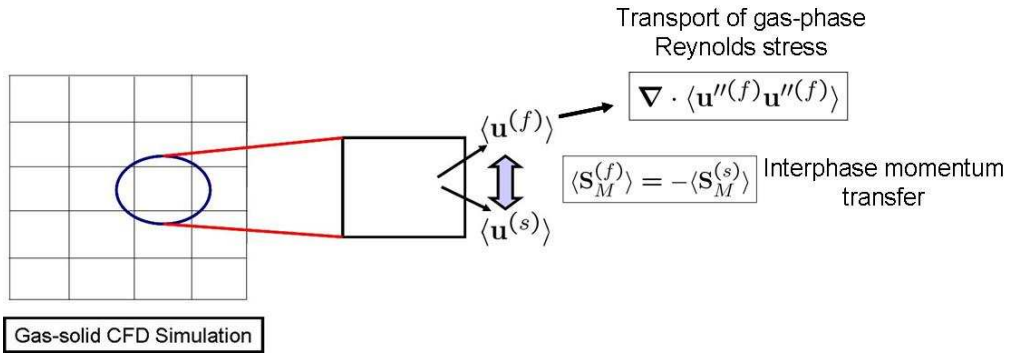

Figure 1: Schematic of a CFD simulation of gas–solid flow. In every computational grid cell, governing equations for the averaged quantities in both phases are solved. Here $\left\langle \mathbf{u}^{(f)} \right\rangle$ is the average gas–phase velocity and $\left\langle \mathbf{u}^{(s)} \right\rangle$ is the average solid–phase velocity. The average interphase momentum transfer $\left\langle \mathbf{S}_M^{(f)} \right\rangle = -\left\langle \mathbf{S}_M^{(s)} \right\rangle$ that represents the coupling between the solid and the gas–phase appears as an unclosed term in both equations. Also, the transport of Reynolds stress in each phase is an unclosed term in the average momentum equation of that phase. Here $\mathbf{u}''^{(f)}$ denotes the fluctuating velocity in the gas–phase.

modeling the unclosed terms that represent interphase interactions. The conservation equation for mean momentum in the gas phase requires models for the average interphase momentum transfer and the transport of the second moments of the fluctuating velocity (Reynolds stress) in the gas phase. The average interphase momentum transfer has been extensively studied and there is a general consensus on drag models (Ergun, 1952; Wen and Yu, 1966; Syamlal, M. and O'Brien, T. J., 1987; Gidaspow, 1994; Hill et al., 2001a,b; van der Hoef et al., 2005; Beetstra et al., 2007; Tenneti et al., 2011). However, the gas–phase Reynolds stress has not been comprehensively quantified in the parameter range corresponding to fluidized beds.

Nevertheless there is some evidence to indicate that gas–phase velocity

fluctuations can be significant. Intrusive hot wire measurements by Moran and Glicksman (2003) indicate that the level of gas–phase velocity fluctuations can be significant in a circulating fluidized bed riser at dilute solid volume fraction. In dense gas–solid flows non–intrusive measurements are difficult because of limited optical access, and the effect of intrusive instrumentation could alter the flow considerably. Although various numerical studies have been performed to understand the effect of particles on the flow turbulence, the vast majority of existing work (Squires and Eaton, 1991; Elghobashi and Truesdell, 1993; Boivin et al., 1998; Sundaram and Collins, 1999; Mashayek and Taulbee, 2002) addresses particle–turbulence interactions with particle diameter D smaller than the Kolmogorov scale of turbulence η. In industrial applications of gas–solids flow such as fluidized beds (Moran and Glicksman, 2003), the particle diameter D is usually larger than the Kolmogorov length scale η. There are relatively few studies (Uhlmann, 2008; Xu and Subramaniam, 2010; Lucci et al., 2011) for particles with $D > \eta$, and but for one study (Xu and Subramaniam, 2010) these focus on flows with nonzero mean slip velocity. Unlike in single–phase turbulence, the mean slip velocity is an important parameter in gas–solid flows with $D > \eta$. Therefore, there is a need to quantify the gas–phase Reynolds stress over a range of solids volume fraction and Reynolds number based on the mean slip velocity between the solid and gas–phase.

In the absence of such comprehensive quantification, the gas–phase Reynolds stress term is sometimes neglected in CFD simulations of dense gas–solid flow on the grounds that the dominant forces in the gas–phase momentum balance are the pressure drop and drag force (Hrenya and Sinclair, 1997). When

models (Benyahia et al., 2005) for the transport of gas–phase Reynolds stress are used, such as in the widely used gas–solid flow CFD code MFIX (Syamlal et al., 1993), these models are simple extensions of single–phase turbulence models that have not been validated in canonical flows. Similarly, due to the lack of data for the gas–phase Reynolds stress at low volume fractions, this term is also neglected in some CFD simulations of dilute gas–solid flow (Agrawal et al., 2001). However, CFD simulations of gas–solid flow in circulating fluidized beds that incorporated a model for the transport of the gas–phase Reynolds stress generally showed good agreement for mean flow velocity profiles with experiments (Bolio et al., 1995; Bolio and Sinclair, 1995; Crowe, 2000; Zhang and Reese, 2003; Benyahia et al., 2005). These observations along with the measurements of Moran and Glicksman (2003) indicate that quantification and modeling of the gas–phase Reynolds stress is necessary.

In some studies (Ahmadi and Ma, 1990b; Bolio and Sinclair, 1995; Balzer et al., 1998; Benyahia et al., 2005) the gas–phase Reynolds stress term is modeled using an eddy viscosity in a fashion similar to single–phase turbulence. However, if the turbulent kinetic energy k_f and the dissipation rate ε_f were quantified in gas–solid flow, one could develop a validated eddy viscosity model. In other works (Ahmadi and Ma, 1990b,a; Bolio and Sinclair, 1995; Balzer et al., 1998; Benyahia et al., 2005) a two–equation approach with transport equations for k_f and ε_f that are modified to account for the presence of solid particles is used. There are also a few studies in which only a transport equation for k_f is solved (one–equation approach) and ε_f is modeled using a Kolmogorov scaling for dissipation (Ahmadi and Ma, 1990b,a;

Kenning and Crowe, 1997; Crowe, 2000). A review of existing multiphase turbulence models can be found in Crowe et al. (1996).

Both the one–equation and two–equation approaches need accurate models for the generation and dissipation rate of k_f. The presence of particles and their changing configuration produces high levels of gas–phase velocity fluctuations, in addition to the turbulent motions already present in the gas phase. In order to account for the generation of gas–phase velocity fluctuations by finite sized particles, Yuan and Michaelides (1992) proposed a model in which the velocity deficit in the wake of the particle is the source and the work done by the drag force is the dissipation of gas velocity fluctuations. Yarin and Hetsroni (1994) employed a similar idea but used a more detailed description of the wake. Although both models showed good agreement with experiments (Tsuji et al., 1984; Modarress et al., 1984), they are not derived by the application of detailed balance laws. Kenning and Crowe (1997) proposed a new turbulence model starting from the conservation equation of mechanical energy in gas–solid flow. In this model, work done by the particle drag force acts as a source for gas–phase velocity fluctuations. Dissipation of gas–phase velocity fluctuations is modeled along the lines of single–phase turbulence($\varepsilon_f \sim k_f^{3/2}/l_{\text{diss}}$). The length scale l_{diss} considered in their work corresponds to a hybrid length scale of inter–particle spacing and the dissipation length scale used in single–phase turbulence. This model was further improved and showed good agreement with experimental data obtained from particle–laden turbulent flow in pipes (Crowe, 2000).

Existing models for the gas–phase Reynolds stress in gas–solid flow that are widely used in CFD calculations are simple extensions of single–phase tur-

bulence models. Most closure models do not distinguish between the velocity fluctuations generated by the presence of particles and inherent turbulence in the flow. This is because both these mechanisms essentially manifest themselves as a non–zero Reynolds stress in the gas–phase. However, because the physical mechanisms resulting in the generation and dissipation of these velocity fluctuations are different, one would expect that their scaling with nondimensional parameters could also be different. This would then imply that models for single–phase turbulence may not be adequate for modeling the pseudo–turbulent velocity fluctuations arising from the presence of particles. For instance, models used for the dissipation of turbulent kinetic energy are based on the Kolmogorov scaling ($k_f^{3/2}/l_{\mathrm{diss}}$) used in single–phase turbulence, but their validity in particle–laden flows is not verified. Furthermore, although two–equation k–ε models are very widely used in CFD of gas–solid flows, the disadvantage of such models is that they cannot account for the anisotropy of the gas–phase Reynolds stress. Recent particle–resolved direct numerical simulation of flow past finite sized particles revealed that the Reynolds stress in the gas–phase is indeed highly anisotropic (Xu and Subramaniam, 2010). This anisotropic Reynolds stress poses additional challenges in modeling gas–solid flows. Anisotropy in the Reynolds stress for the case of inherent turbulence in gas–solid flow with $D < \eta$ has been accounted for in some recent models (Wang et al., 1998).

In this study we use direct numerical simulation to address these outstanding questions related to gas–phase velocity fluctuations in gas–solid flow. A popular numerical approach is the *point particle* direct numerical simulation methodology (Squires and Eaton, 1991; Elghobashi and Trues-

dell, 1993; Boivin et al., 1998; Sundaram and Collins, 1999; Mashayek and Taulbee, 2002) (DNS) in which the particles are treated as points and the effect of the particles on the gas–phase is represented by a force applied at the particle center. This approach is valid only when the particle size is much smaller compared to the Kolmogorov length scale. When the particle size is larger or comparable to the Kolmogorov length scale, the effects of the wake generated by the particles become important and hence it is important to resolve the boundary layers around the particle. For particles of size comparable to or larger than the Kolmogorov length scale, the appropriate numerical approach is the particle–resolved direct numerical simulation (PR–DNS) methodology in which all the scales of the inherent turbulence and the flow scales introduced by the presence of large particles are resolved. PR–DNS has been used to study the interaction of a single particle with decaying homogeneous isotropic turbulence (Bagchi and Balachandar, 2003; Burton and Eaton, 2005). PR–DNS has also been employed to study the effect of a collection of particles on decaying homogeneous isotropic turbulence (Lucci et al., 2011), particle–laden turbulent channel flow(Uhlmann, 2008) as well as gas–solid flow with upstream turbulence (Xu and Subramaniam, 2010). In fact, understanding the generation of gas–phase velocity fluctuations using PR–DNS has been identified as one of the future directions in the review article by Balachandar and Eaton (2010). Therefore, PR–DNS is appropriate to characterize the level of gas–phase velocity fluctuations in gas–solid suspensions of large, high Stokes number particles over a wide range of solid volume fraction and Reynolds number based on the mean gas–solid slip velocity.

We use PR–DNS to quantify the strength of gas–phase velocity fluctuations and the state of anisotropy of the gas–phase Reynolds stress tensor in steady flow through a statistically homogeneous fixed assembly of monodisperse spheres. To differentiate between the gas–phase velocity fluctuations generated by the presence of particles and the inherent turbulence present in the flow field, we consider "laminar" gas–solids flow in this work. In the context of this work, "laminar" flow implies that there is no inherent turbulence in the flow field i.e. in the absence of particles, the flow field is not turbulent. In fixed–bed simulations the particles are held stationary and a steady flow is established by imposing a pressure gradient that corresponds to the desired flow rate. Use of the fixed–bed simulation methodology for gas–solid flows is justified if the configuration of the particles changes very slowly compared to the time it takes to attain mean momentum balance. The time scale over which the particle configuration changes depends on $\mathrm{Re}_T = DT^{1/2}/\nu_f$, which is the Reynolds number based on the particle fluctuating velocity that is characterized by the particle granular temperature T. Particle–resolved simulations of freely evolving suspensions (Tenneti et al., 2010) and recent high–speed imaging of particles (Cocco et al., 2010) show that this value of Re_T is low for high Stokes number suspensions. Moreover, using PR–DNS, Mehrabadi et al. (2012) observed that the level of gas–phase velocity fluctuations observed in freely evolving suspensions is close to that observed in fixed particle assemblies. The fixed–bed simulation setup has been used successfully to extract computational drag laws (Hill et al., 2001a,b; van der Hoef et al., 2005; Beetstra et al., 2007; Tenneti et al., 2011) as well as to understand the effect of particle clusters on gas–phase turbulence (Xu and

Subramaniam, 2010). Using the data obtained from PR–DNS, we analyze the implications for modeling the dissipation rate of kinetic energy in the gas–phase by considering the energy balance equation similar to the work of Kenning and Crowe (1997). We also use the particle–resolved DNS data to propose an eddy viscosity for gas–solid flow in terms of solid volume fraction and mean flow Reynolds number.

The rest of the paper is organized as follows. In section 2 we define the ensemble–averaged quantities that are computed from PR–DNS. We briefly describe our PR–DNS approach and its validation in sections 3 and 4, respectively. The results quantifying the strength of gas–phase velocity fluctuations and anisotropy of gas–phase Reynolds stress in terms of solid volume fraction and mean flow Reynolds number are presented in section 6. The multiphase turbulence model derived using a simple scaling analysis is described in section 7. An eddy viscosity model for gas–solid flow is proposed in section 8, followed by the conclusions in section 9.

2. Gas–phase velocity variance

In the Eulerian two-fluid theory, the fluid–phase Reynolds stress is defined as a phasic average, which is an average conditional on the presence of the fluid phase Drew (1983); Drew and Passman (1998); Pai and Subramaniam (2009). If $Q(\mathbf{x},t)$ is any field, then its phasic average $\left\langle Q^{(f)}\right\rangle(\mathbf{x},t)$ referred to as its fluid–phase mean, is defined as:

$$\left\langle Q^{(f)}\right\rangle(\mathbf{x},t)=\frac{\left\langle I_{\mathrm{f}}(\mathbf{x},t)\,Q(\mathbf{x},t)\right\rangle}{\left\langle I_{\mathrm{f}}(\mathbf{x},t)\right\rangle}. \tag{1}$$

Here the fluid–phase indicator function I_f is unity if the point $\mathbf{x}$ lies in the fluid–phase and zero otherwise.

Using this definition, the ensemble–averaged kinetic energy in the fluid phase $\left\langle E^{(f)} \right\rangle$ is defined as

$$\left\langle E^{(f)} \right\rangle = \frac{1}{2} \frac{\langle I_f u_i u_i \rangle}{\langle I_f \rangle}, \tag{2}$$

where $\mathbf{u}$ is the fluid velocity. It is easy to see that the average kinetic energy in the fluid phase is the sum of the kinetic energy in the mean fluid motion E_f and the average kinetic energy in the fluctuating motions k_f. The average kinetic energy in the mean fluid motion is given by $E_f = \frac{1}{2} \left\langle u_i^{(f)} \right\rangle \left\langle u_i^{(f)} \right\rangle$, where the quantity $\left\langle u_i^{(f)} \right\rangle$ is the phase–averaged fluid velocity. The average kinetic energy in the fluctuating motion of the fluid is given by

$$k_f = \frac{1}{2} \frac{\left\langle I_f u_i^{\prime\prime(f)} u_i^{\prime\prime(f)} \right\rangle}{\langle I_f \rangle}, \tag{3}$$

where fluctuations in the fluid velocity field are defined with respect to the phase–averaged fluid velocity i.e., $u_i^{\prime\prime(f)} = u_i - \left\langle u_i^{(f)} \right\rangle$. We now describe how k_f is computed from solution of flow past statistically homogeneous suspensions using particle–resolved DNS.

2.1. Quantifying gas–phase velocity variance from particle–resolved DNS

In PR–DNS a single realization from the ensemble of events that contribute to the phasic average in Eq. 3 is simulated (cf. Fig. 2). Here we describe how PR–DNS data from multiple realizations is used to compute k_f. Let $\mathbf{u}\left(\mathbf{x}, t; \omega\right)$ be the velocity field obtained from particle–resolved DNS of flow past a random configuration of particles represented by the positions and velocities $\left\{\mathbf{X}^{(i)}, \mathbf{V}^{(i)}, i = 1, \ldots, N_p\right\}$ of N_p particles. This configuration represents a realization ω in the event space Ω. The ensemble–averaged velocity field or the mathematical expectation is defined as (Subramaniam,

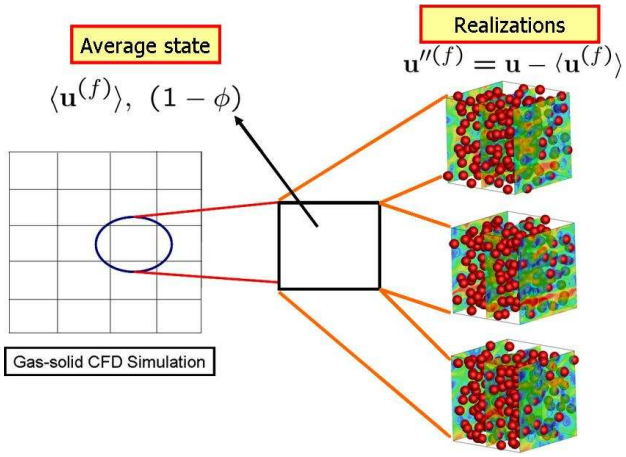

Figure 2: Schematic showing the concept of the average fluid–phase velocity. The average fluid–phase velocity that is solved in gas–solid CFD simulations is obtained by averaging over all possible realizations.

2000):

$$\langle \mathbf{u} \rangle (\mathbf{x}, t) = \int_{\Omega} \mathbf{u} (\mathbf{x}, t; \omega)\ dP_{\omega}, \tag{4}$$

where P_{ω} is the probability measure that is defined on Ω. This concept is explained schematically in Fig. 2. The average gas–phase velocity and volume fraction that are solved in the CFD calculations are obtained by averaging over all possible realizations. Fluctuations in the gas–phase velocity are defined as departures of the instantaneous velocity field from the average gas–phase velocity.

If the flow is statistically homogeneous, ensemble–averaged quantities can be approximated by taking the volumetric mean of the solution fields, e.g. the volumetric mean of the velocity field over the fluid region is defined as:

$$\left\langle \mathbf{u}^{(f)} \right\rangle_{\mathcal{V}} (t; \omega) = \frac{1}{V_f} \int_{\mathcal{V}} I_f (\mathbf{x}, t; \omega)\, \mathbf{u} (\mathbf{x}, t; \omega) dV, \tag{5}$$

where V_f is the volume of the region occupied by the fluid–phase. It has been shown elsewhere (Tenneti et al., 2011) that a statistically homogeneous gas–solid flow is well approximated by flow past a random configuration of particles in a periodically repeating unit cell. Therefore, volume averages can be used to estimate the true mathematical expectation. The volumetric mean approaches the ensemble average in the limit of infinite box size (i.e., $V \to \infty$). Periodic bounday conditions can be used in a computational domain with finite box size provided the two–point correlations in the particle and the fluid phases decay to zero within the box length[1]. In Section 5 we show that the Eulerian two–point correlation of fluid velocity does indeed decay to zero within 3 to 4 particle diameters for different grid resolutions, box sizes and Reynolds numbers. However, a finite box may not account for the statistical variability arising from different particle configurations, we require very large box sizes. In order to accurately estimate the ensemble–averaged quantities from finite box sizes, we can simulate fixed particle assemblies and average over different configurations. For fixed particle assemblies, the ensemble–average can be estimated by averaging over different configurations or realizations i.e.,

$$\left\{\mathbf{u}^{(f)}\right\}_{\mathcal{V},\mathcal{M}}(t) = \frac{1}{\mathcal{M}}\sum_{\mu=1}^{\mathcal{M}} \left\langle \mathbf{u}^{(f)} \right\rangle_{\mathcal{V}}(t;\omega_\mu). \tag{6}$$

In the above equation $\left\{\mathbf{u}^{(f)}\right\}_{\mathcal{V},\mathcal{M}}$ denotes an estimate to the true expectation $\left\langle \mathbf{u}^{(f)} \right\rangle$ and $\mathcal{M}$ denotes the number of independent realizations. Similarly, for each realization of the gas–solid flow we compute the kinetic energy in the

[1]This is simply the two–phase extension of the criterion given by Pope (2000) for single–phase turbulent flows.

fluctuating motions using volume averaging:

$$k_f^{(\mu)} = \frac{1}{V_f} \int\limits_{\mathcal{V}_{\mathrm{f}}^{(\mu)}} \frac{1}{2} \left(\mathbf{u}\left(\mathbf{x}, t, \omega_\mu\right) - \left\{ \mathbf{u}^{(f)} \right\}_{\mathcal{V},\mathcal{M}} \right) \cdot \left(\mathbf{u}\left(\mathbf{x}, t, \omega_\mu\right) - \left\{ \mathbf{u}^{(f)} \right\}_{\mathcal{V},\mathcal{M}} \right) \, dV. \tag{7}$$

The k_f obtained from a single realization (cf. 7) is averaged over multiple independent realizations (MIS) to obtain an estimate for the ensemble-averaged kinetic energy:

$$k_f = \frac{1}{\mathcal{M}} \sum_{\mu=1}^{\mathcal{M}} k_f^{(\mu)}. \tag{8}$$

In the next section we describe the particle–resolved DNS approach that is used in this work to quantify k_f in steady flow past fixed assemblies of spheres.

3. Numerical Method

The particle–resolved DNS methodology employed in this work is called Particle–resolved Uncontaminated–fluid Reconcilable Immersed Boundary Method (PUReIBM). In PUReIBM, we employ Cartesian grids and solve the mass and momentum conservation equations on all the grid points (including those lying inside the particles). A fictitious flow is generated inside the particles that does not affect the exterior flow solution. The mass and momentum conservation equations that are solved in PUReIBM are

$$\frac{\partial u_i}{\partial x_i} = 0 \ , \tag{9}$$

and

$$\rho_f \frac{\partial u_i}{\partial t} + \rho_f S_i = -g_{\mathrm{IBM},i} + \mu_f \frac{\partial^2 u_i}{\partial x_j \partial x_j} + f_{\mathrm{u},i}, \tag{10}$$

respectively, where $\mathbf{g}_{\mathrm{IBM}}$ is the pressure gradient, $\mathbf{S} = \boldsymbol{\nabla} \cdot (\mathbf{uu})$ is the convective term in conservative form, and $\mathbf{u}$ is the instantaneous velocity field. In Eq. (10), $\mathbf{f}_{\mathrm{u}}$ is the additional immersed boundary (IB) force term that accounts for the presence of solid particles by ensuring the no–slip and no–penetration boundary conditions at the particle–fluid interface.

The surface of the solid particle is represented by a discrete number of points called boundary points. For spherical particles, the boundary points are specified by discretizing the sphere in spherical coordinates. In Fig. 3, a schematic describing the computation of the IB forcing is shown for the equatorial plane passing through the spherical particle. Another set of points called exterior points are generated by projecting these boundary points onto a sphere of radius $r + \Delta r$, where r is the radius of the particle (see exterior point represented by an open circle on the dashed line in Fig. 3). Similarly, the boundary points are projected onto a smaller sphere of radius $r - \Delta r$ and these points are called interior points. In our simulations Δr is taken to be same as the grid spacing. The IB force is computed at the interior points. At these points the fluid velocity is forced in a manner similar to the ghost cell approach used in standard finite-difference/finite-volume based methods (Patankar, 1980). Specifically for the case of zero solid particle velocity, the velocity at the interior points is forced to be equal in magnitude but opposite in direction of the fluid velocity at the corresponding exterior points. Velocities at the exterior and interior points are obtained by interpolating the velocities from the neighboring grid nodes. The computation of IB forcing is similar to the direct forcing method proposed by Yusof (1996). The IB forcing at the $(n+1)^{\mathrm{th}}$ time-step is specified to cancel the remaining terms

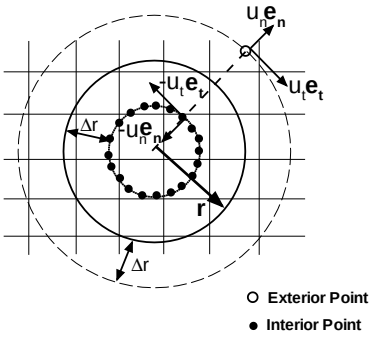

Figure 3: A schematic showing the computation of the immersed boundary forcing for a stationary particle. The solid circle represents the surface of the particle at r. Open dot shows the location of one exterior point at $r + \Delta r$ (only one exterior point is shown for clarity, although there is one exterior point for each interior point) and filled dots show the location of interior points at $r - \Delta r$ where the immersed boundary forcing is computed. For the special case of a stationary particle, the velocity at the interior points is forced to be the opposite of the velocity at the corresponding exterior points. In the schematic, $u_n \mathbf{e}_n$ represents the normal velocity and $u_t \mathbf{e}_t$ represents the tangential velocity at the exterior point.

in the momentum conservation, and to force the velocity to its desired value $\mathbf{u}^d$ at the interior points:

$$f_{\mathrm{u},i}^{n+1} = \rho_f \frac{u_i^d - u_i^n}{\Delta t} + \rho_f S_i^n + g_{\mathrm{IBM},i}^n - \mu_f \frac{\partial^2}{\partial x_j \partial x_j} u_i^n. \tag{11}$$

The IB forcing at the interior points is then interpolated to the neighboring grid nodes that do not include grid nodes in the fluid phase. It is noteworthy that the discretization of the sphere in spherical coordinates is independent of the grid resolution and hence to some extent, decouples the grid resolution from the accuracy with which the boundary condition is imposed.

The governing equations in PUReIBM are solved by imposing periodic boundary conditions on fluctuating variables that are now defined. The velocity field is decomposed into a spatially uniform mean flow that is purely time–dependent and a fluctuating velocity field $\mathbf{u}'$ that is periodic, i.e.,

$$\mathbf{u}\left(\mathbf{x}, t\right) = \left\langle \mathbf{u} \right\rangle_{\mathcal{V}}\left(t\right) + \mathbf{u}'\left(\mathbf{x}, t\right), \tag{12}$$

where the volumetric mean velocity

$$\left\langle \mathbf{u} \right\rangle_{\mathcal{V}}\left(t\right) = \frac{1}{V} \int\limits_{\mathcal{V}} \mathbf{u}\left(\mathbf{x}, t\right) d\mathcal{V}, \tag{13}$$

is obtained by averaging the velocity field over the entire computational domain. Similar decompositions can be written for the non-linear term $\mathbf{S}$, pressure gradient $\mathbf{g}$, and immersed boundary forcing $\mathbf{f}_{\mathrm{u}}$ terms. Substituting the above decompositions in Eqs. (9) and (10), followed by averaging over the entire computational domain yields the volume averaged mass and momentum conservation equations. Since the volumetric means are independent of spatial location, mean mass conservation is trivially satisfied. The mean

momentum balance in the whole domain is

$$\rho_f \frac{d\langle u_i \rangle_{\mathcal{V}}}{dt} = -\langle g_{\mathrm{IBM},i} \rangle_{\mathcal{V}} + \langle f_{\mathrm{u},i} \rangle_{\mathcal{V}}, \tag{14}$$

where the volume integrals of convective and diffusive terms are zero because of periodic boundary conditions. The mean IB forcing term $\langle \mathbf{f}_{\mathrm{u}} \rangle_{\mathcal{V}}$ is computed by volume–averaging the IB force specified by Eq. 11 over the region $\mathcal{V}$. The mean pressure gradient $\langle \mathbf{g}_{\mathrm{IBM}} \rangle_{\mathcal{V}}$ is computed such that we obtain the desired flow rate.

Evolution equations for the fluctuating variables are derived by subtracting Eq. (14) from Eq. (10). The resulting equations are solved using a pseudo-spectral method, with Crank-Nicolson scheme for the viscous terms, and an Adams-Bashforth scheme for the convective terms. A fractional time-stepping method that is based on Kim and Moin's approach (Kim and Moin, 1985) is used to advance the fluctuating velocity fields in time. The principal advantage of the PUReIBM approach is that it enables the use of regular Cartesian grids to solve for flow past arbitrarily shaped moving bodies without the need for costly remeshing.

The salient features that distinguish PUReIBM from other immersed boundary method approaches (including the original implementation of Yusof (1996)) are as follows:

1. Uncontaminated fluid: In PUReIBM the immersed boundary (IB) forcing is solely restricted to those grid points that lie in the solid phase, and therefore the flow solution in the fluid phase is uncontaminated by the IB forcing. Consequently the velocity and pressure in the fluid phase is a solution to the unmodified Navier-Stokes equations (in contrast to IB implementations that smear the IB forcing on to grid points

in the fluid phase adjoining solid boundaries, resulting in solution fields that do not correspond to unmodified Navier–Stokes equations).

2. Reconcilable: In PUReIBM the hydrodynamic force experienced by a particle is computed directly from the stress tensor at the particle surface that is obtained from this uncontaminated fluid flow solution (in contrast to IB implementations that calculate the hydrodynamic force from the IB forcing field). This feature of PUReIBM enables us to directly compare the DNS solution with any random-field theory of multiphase flow.

4. Validation

The PUReIBM PR–DNS methodology has been extensively validated (Garg et al., 2010b; Tenneti et al., 2011) by comparing the drag force obtained from PUReIBM with available experimental and simulation data in the literature in a comprehensive suite of test cases:

1. Drag acting on a single sphere (Garg et al., 2010b; Garg, 2009) with experimental correlation of Schiller and Nauman (1935)
2. Drag acting on simple cubic and face centered cubic arrangements (Tenneti et al., 2011) of particles in Stokes flow regime with those reported by Zick and Homsy (1982) using the Boundary Integral method (semi–analytic solution)
3. Drag acting on simple cubic (SC) and face centered cubic (FCC) arrangements (Tenneti et al., 2011) of particles at moderate Reynolds numbers with the results published by Hill et al. (2001b) using lattice Boltzmann method (LBM)

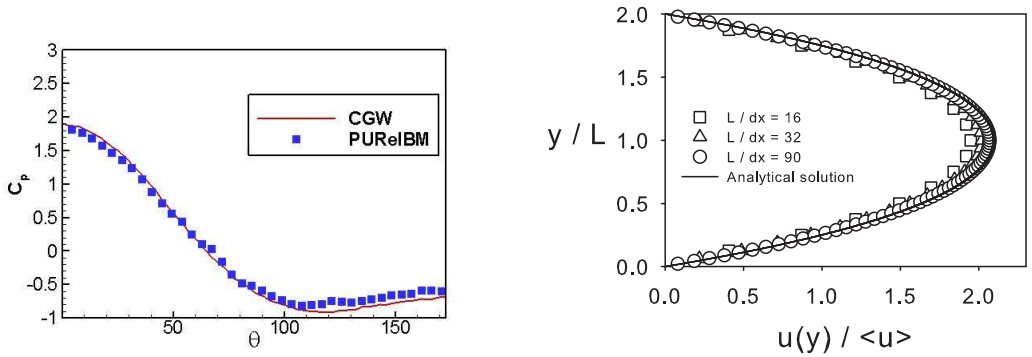

(a) (b)

Figure 4: (a) Variation of the coefficient of pressure C_p along the surface of the sphere. Symbols are the data obtained from PUReIBM simulations for a Reynolds number of 10, while the solid line is that reported in the book authored by Clift, Grace and Weber (CGW) Clift et al. (1978). (b) Comparison of the velocity profile in a square duct obtained from PUReIBM simulations at a Reynolds number of 20 with analytical solution Cornish (1928). It is worthwhile to note that the walls are generated using the immersed boundary method.

4. Mean drag acting on a random arrangement Tenneti et al. (2011) of particles in the Stokes flow regime with the results published by Hill et al. (2001a) and van der Hoef et al. (2005) using LBM
5. High Reynolds number flow past random arrays of monodisperse spheres with ANSYS–FLUENT CFD package

In addition to the comprehensive validation of the PUReIBM method (Tenneti et al., 2011; Garg et al., 2010b) , we present selected additional validation tests to establish the numerical convergence and accuracy of PUReIBM near solid boundaries in Fig. 4. The first plot (see Fig. 4(a)) shows a comparison of the pressure coefficient along the surface of a sphere obtained from our

PR–DNS with that reported in the book of Clift et al. (1978) (CGW) for an isolated sphere at a Reynolds number of 10. Figure 4(a) shows an excellent agreement of the pressure profile on the surface of the sphere with the data reported in CGW. The second plot (see Fig. 4(b)) shows a comparison of the velocity field in a square duct at a Reynolds number of 20 with the analytical solution given by Cornish (1928). We can see that the velocity profile obtained from PUReIBM is numerically converged and accurate. These plots show that in addition to getting the total drag correct, our method computes the correct contributions of pressure and viscous drag forces. In the following section we describe the simulation setup used to compute the level of gas–phase velocity fluctuations and also discuss the choice of the numerical parameters needed to ensure numerically converged results.

5. Simulation Setup

In our simulation setup the particles are held stationary and a steady flow is established by imposing a pressure gradient that corresponds to the desired mean flow Reynolds number. A typical simulation of flow past random arrangement of particles with contours of local kinetic energy ($k^{(f)} = \frac{1}{2} u_i''^{(f)} u_i''^{(f)}$) normalized by the mean energy are shown in Fig. 5. In all the simulations, mean flow is directed along the positive x–axis.

For flow past homogeneous particle assemblies, a Reynolds number based on the magnitude of mean slip velocity between the two phases is defined as

$$\mathrm{Re}_m = \frac{|\langle \mathbf{W} \rangle| \, (1-\phi) \; D}{\nu_f}, \tag{15}$$

where $|\langle \mathbf{W} \rangle|$ is the magnitude of the mean slip velocity, D is the particle diameter and ϕ is the solid volume fraction. The mean slip velocity $\langle \mathbf{W} \rangle =$

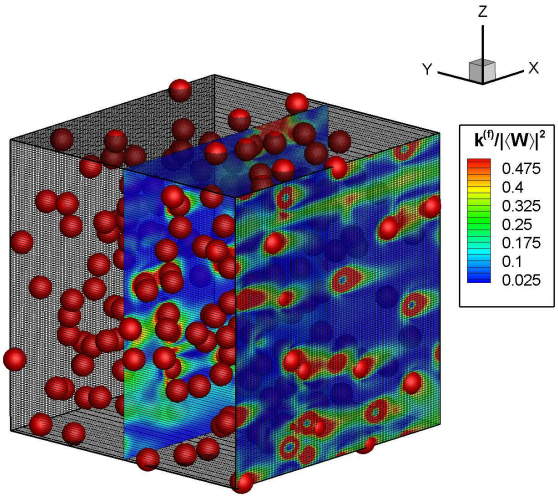

Figure 5: Contours of local kinetic energy ($k^{(f)} = \frac{1}{2} u_i''^{(f)} u_i''^{(f)}$) in the gas–phase normalized by the mean energy for steady flow past random assembly of spheres at a solid volume fraction of 0.05 and mean flow Reynolds number of 50.

$\left\langle \mathbf{u}^{(s)} \right\rangle - \left\langle \mathbf{u}^{(f)} \right\rangle$ is defined as the difference between the average solid and gas–phase velocities. In the simulations, the mean flow Reynolds number (or the desired flow rate) is specified as an input and since for fixed assemblies $\left\langle \mathbf{u}^{(s)} \right\rangle = 0$, the desired fluid-phase mean velocity $\left\langle \mathbf{u}^{(f)} \right\rangle$ is known in terms of the input Reynolds number and other physical properties. The mean pressure gradient evolves in time until it attains the value required to drive the fluid at the desired flow rate.

Particles are initialized corresponding to a specified mean solid volume fraction ϕ. The particles are fixed in a random equilibrium configuration they attain following elastic collisions (in the absence of ambient fluid) starting from a lattice arrangement with a Maxwellian velocity distribution. The elastic collisions are simulated using a soft–sphere discrete element model (Cun-

dall and Strack, 1979; Garg et al., 2010a). The pair correlation function at equilibrium specifies the particle configuration for random assemblies.

The computational domain used is a cube with sides of length L which is discretized using a regular Cartesian grid with M grid cells in each direction so that $\Delta x = L/M$ is the size of each grid cell. The spatial resolution is represented by the number of grid cells across the diameter of a particle, which is denoted $D_m = D/\Delta x$. For random arrangements of particles, the ratio L/D is an independent parameter. The minimum box length is determined by the criterion that the spatial autocorrelation of flow statistics must decay to zero within the box. This is to prevent the periodicity of the numerical solution from leading to unphysical flow fields. The numerical parameter L/D also determines the number of particles N_p in the box such that for a given volume fraction ϕ it is given by

$$N_p = \frac{6\phi}{\pi}\left(\frac{L}{D}\right)^3. \tag{16}$$

The various numerical parameters used in the simulations are reported in Table 1.

All simulations start with the initial condition of uniform fluid velocity. We have verified that starting the simulations with a homogeneous isotropic turbulent velocity field does not affect the steady value of k_f attained by the system (Mehrabadi et al., 2012). Therefore the steady state value of k_f obtained in a fixed particle assembly depends only on the solids volume fraction and the mean flow Reynolds number. The grid resolutions used in the PUReIBM simulations have been chosen such that they yield numerically converged solutions. For instance, the convergence characteristics of k_f/E_f with respect to the grid resolution D_m for a solid volume fraction of 0.3 and

ϕ	N_p	$\mathcal{M}$	D_m	L/D
0.1	80/ 41	5	20/30	7.5/ 6
0.2	161/ 34	5	20/40	7.5/ 4.5
0.3	71/ 26	5	30/50	5/ 3.6
0.4	95/ 20	5	30/60	5/ 3
0.5	61/–	5	40/–	4/–

Table 1: Numerical parameters (number of particles N_p, number of MIS $\mathcal{M}$, particle diameter in grid units D_m and the ratio of the length of the box to the particle diameter L/D) used for random arrays in PUReIBM simulations. Different numerical parameters are used for $\mathrm{Re}_m \leq 100$ and $\mathrm{Re}_m > 100$. These are separated by "/". Numbers before the "/" correspond to $\mathrm{Re}_m \leq 100$ while numbers after the "/" correspond to $\mathrm{Re}_m > 100$. At volume fraction 0.5 PUReIBM simulations are performed only up to a Reynolds number of 100.

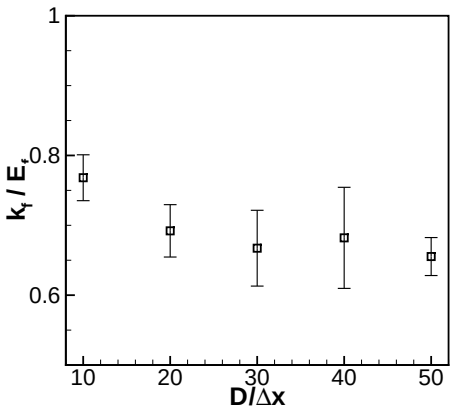

Figure 6: Convergence characteristics of k_f/E_f with grid resolution $D/\Delta x$ for flow past random arrays of spheres at $\phi = 0.3$ and $\mathrm{Re}_m = 20$. The error bars denote 95% confidence intervals in the estimation of the average k_f from 5 independent realizations.

mean flow Reynolds number of 20 is shown in Fig. 6. The value of k_f/E_f averaged over 5 independent realizations clearly shows numerical convergence as the grid resolution is increased.

Besides convergence with grid resolution, it is also important to check whether the box size is adequate or not. The box size is deemed adequate if the two–point correlation functions in the fluid–phase decay to zero within the box length. To check this, the two–point velocity correlation function has been computed for the highest Reynolds number simulated. The fluid–phase velocity autocorrelation $\rho_u(r)$ is defined as

$$\rho_u(r) = \frac{\left\langle I_f(\mathbf{x})\,\mathbf{u}''^{(f)}(\mathbf{x}) \cdot I_f(\mathbf{x}+\mathbf{r})\,\mathbf{u}''^{(f)}(\mathbf{x}+\mathbf{r})\right\rangle}{\left\langle I_f \mathbf{u}''^{(f)} \cdot \mathbf{u}''^{(f)}\right\rangle}. \tag{17}$$

Figure 7(a) shows convergence of the fluid–phase velocity autocorrelation function with grid resolution as well as box size for a random configuration of particles at a solid volume fraction of 0.2 and Reynolds number of 20. The

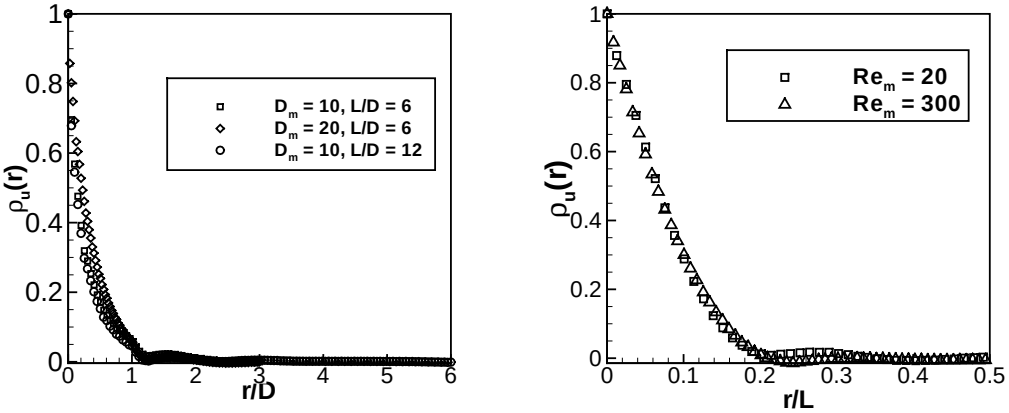

(a) (b)

Figure 7: (a) Convergence of the fluid–phase velocity autocorrelation function with grid resolution as well as box size for a random configuration of particles at a solid volume fraction of 0.2 and Reynolds number of 20. (b) Decay of the fluid velocity autocorrelation function obtained from PUReIBM simulation of steady flow past a random configuration of spheres at a solid volume fraction of 0.2 and mean flow Reynolds numbers 20 (squares) and 300 (triangles). In these simulations L/D ratios of 6 and 4.5 are used for Reynolds numbers 20 and 300 respectively.

autocorrelation function has also been computed for the highest Reynolds number that we simulated and is shown in Fig. 7(b). These results clearly indicate that the numerical parameters used in our simulation are adequate to perform numerically converged simulations. We now present the results obtained from PUReIBM simulations of flow past monodisperse fixed particle assemblies.

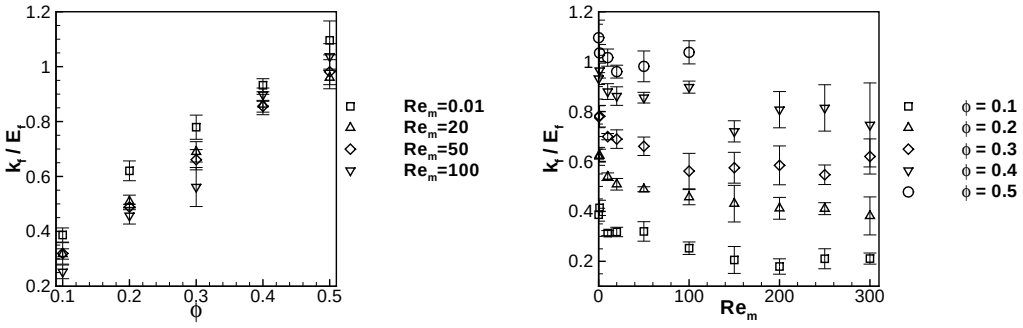

(a) (b)

Figure 8: Variation of the turbulent kinetic energy normalized by $E_f = \frac{1}{2}\left\langle \mathbf{u}^{(f)} \right\rangle \cdot \left\langle \mathbf{u}^{(f)} \right\rangle$ with Re_m and ϕ.Figure 8(a) shows the behavior of k_f/E_f with ϕ for different mean flow Reynolds numbers while Fig. 8(b) shows the behavior of k_f/E_f with Re_m for different solid volume fractions.

6. Results

We performed PUReIBM DNS of flow past fixed assemblies of monodisperse spheres over a wide range of solids volume fraction ($0.1 \leq \phi \leq 0.5$) and mean flow Reynolds numbers ($0.01 \leq \mathrm{Re}_m \leq 300$). Using this data a new correlation for the average fluid–particle force in fixed beds has been proposed by Tenneti et al. (2011). Here we quantify the strength of gas–phase velocity fluctuations in terms of ϕ and Re_m.

Figure 8(a) shows the variation of k_f/E_f with solids volume fraction for different mean flow Reynolds numbers while Fig. 8(b) shows the variation of k_f/E_f with mean flow Reynolds number for different solid volume fractions. As evident from Fig. 8(a), the kinetic energy in fluctuating motions normalized by the mean energy in the gas–phase increases dramatically with volume fraction. This behavior is expected because, as the volume fraction

increases, the space available to the gas decreases. Owing to conservation of mass, the velocity of the gas increases thus causing k_f/E_f to increase with volume fraction. As shown in Fig. 8(b), at a given volume fraction k_f/E_f decreases rapidly with increasing mean flow Reynolds number up to $\mathrm{Re}_m = 50$ and beyond $\mathrm{Re}_m = 50$ it has a weak power law dependence on Re_m. This behavior is a result of the normalization of k_f by E_f. It implies that the variance of gas velocity increases approximately as the square of the mean flow Reynolds number. Since the total kinetic energy of the gas increases with increasing mean flow Reynolds number, we expect the strength of gas–phase velocity fluctuations also to increase. Using the data obtained from PUReIBM DNS we found that the following function fits the data with an average deviation of 5%:

$$\frac{k_f}{E_f}\left(\phi, \mathrm{Re}_m\right) = 2\phi + 2.5\phi(1-\phi)^3 \exp\left(-\phi \mathrm{Re}_m^{1/2}\right), \quad 0.1 \leq \phi \leq 0.5, \quad 0.01 \leq \mathrm{Re}_m \leq 300. \tag{18}$$

As shown in Eq. 18, the correlation is proposed from simulations in the range $0.1 \leq \phi \leq 0.5$ and $0.01 \leq \mathrm{Re}_m \leq 300$. The value of k_f/E_f from Eq. (18) tends to appropriate values in the limit of infinite dilution and creeping flow. In the limiting case of infinite dilution i.e. $\phi \to 0$ the value of k_f/E_f is zero. This limiting value is consistent with the fact that in the absence of particles the flow field is uniform. In the Stokes flow regime ($\mathrm{Re}_m \to 0$) the value of k_f/E_f reaches an asymptote and depends only on the solid volume fraction. This behavior is consistent with the fact that the mean drag (which is shown to be the source of k_f in the next section) acting on the particles is linear in the Stokes flow regime and thus the normalized quantity k_f/E_f is

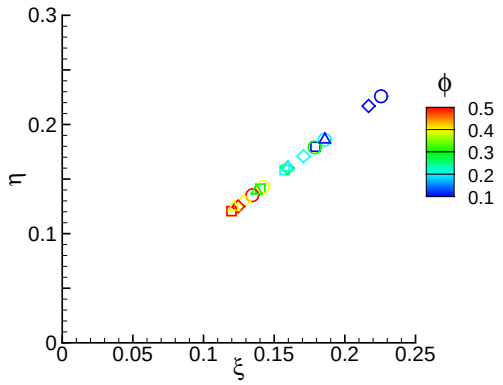

Figure 9: State of anisotropy of the gas–phase Reynolds stress tensor in the Lumley plane. Color of the symbol indicates the volume fraction going from $\phi = 0.1$ (blue) to $\phi = 0.5$ (red). For each volume fraction the invariants of the gas–phase Reynolds stress tensor are shown: $\mathrm{Re}_m = 0.01$ (squares), $\mathrm{Re}_m = 20$ (circles), $\mathrm{Re}_m = 100$ (diamonds) and $\mathrm{Re}_m = 200$ (triangles) are shown.

independent of Reynolds number.

In addition to k_f we also quantified the state of anisotropy of the fluid phase Reynolds stress tensor. To quantify the state of anisotropy of the fluid phase Reynolds stress, the invariants ξ and η of the normalized Reynolds stress anisotropy tensor, which is defined as

$$b_{ij} = \frac{1}{2k_f} \left\langle I_f {u_i}''^{(f)} {u_j}''^{(f)} \right\rangle - \frac{1}{3}\delta_{ij},$$

are computed. The invariants are defined following Lumley and Newman (1977) as $6\eta^2 = b_{ij}b_{ij}$ and $6\xi^3 = b_{ij}b_{jk}b_{ki}$. The state of anisotropy of the gas–phase Reynolds stress tensor for various volume fractions and mean flow Reynolds number is plotted on the ξ–η plane in Fig. 9. The key finding here is that at every Reynolds number the level of anisotropy decreases with increasing volume fraction. In other words, the gas–phase Reynolds stress

tensor is more anisotropic at dilute volume fractions than at denser volume fractions.

Although our study is for homogeneous gas–solid suspensions, the dependence of k_f on the solid volume fraction and mean flow Reynolds number has implications for transport of the gas–phase Reynolds stress in inhomogeneous flows also. The strong dependence of k_f on ϕ suggests that the transport of k_f could be significant in statistically inhomogeneous flows with spatial variation of ϕ. Moreover, the dependence of k_f on ϕ and Re_m (cf. Eq. (18)) obtained in this section has certain implications for modeling the dissipation of kinetic energy in the gas–phase, which are discussed in the following section by employing a scaling analysis.

7. Implications for modeling the dissipation of kinetic energy

In this simple flow the steady k_f results from a balance of interphase transfer of kinetic energy and dissipation of kinetic energy in the gas–phase. If we are able to obtain the correct scaling of each of these terms with ϕ and Re_m then we can explain the dependence of k_f on ϕ and Re_m. For statistically homogeneous flows the conservation law (Pai and Subramaniam, 2009; Ying and Subramaniam, 2007) for k_f is:

$$\frac{\partial}{\partial t}\{(1-\phi)\,\rho_f k_f\} = -\left\langle {u_i}''^{(f)} \tau_{ji} n_j^{(s)} \delta\left(\mathbf{x}-\mathbf{x}^{(I)}\right)\right\rangle + \left\langle {u_i}''^{(f)} \frac{\partial\left(I_f \tau_{ji}\right)}{\partial x_j}\right\rangle . \quad (19)$$

In this equation τ_{ji} is the fluid phase stress tensor (cf. Appendix A), $\delta\left(\mathbf{x}-\mathbf{x}^{(I)}\right)$ is a generalized delta function at the fluid–particle interface $\mathbf{x}^{(I)}$, and $\mathbf{n}^{(s)}$ is the unit normal vector pointing outward from the solid phase into the fluid phase. The second term on the right hand side is the covariance

of the fluctuating fluid velocity field and the gradient of the stress tensor in the fluid phase. For statistically homogeneous flows this term simplifies (cf. Appendix Appendix A) to $-2\mu_f \langle I_f s_{ij} s_{ij} \rangle$, where $2\mu_f \langle I_f s_{ij} s_{ij} \rangle$ can be identified as the dissipation that is strictly non negative. Thus the conservation equation for k_f simplifies to

$$\frac{\partial}{\partial t}\{(1-\phi)\,\rho_f k_f\} = -\left\langle {u_i}''^{(f)} \tau_{ji} n_j^{(s)} \delta\left(\mathbf{x}-\mathbf{x}^{(I)}\right)\right\rangle - 2\mu_f \langle I_f s_{ij} s_{ij}\rangle\,. \tag{20}$$

Here $s_{ij} = \dfrac{1}{2}\left(\dfrac{\partial {u_i}''^{(f)}}{\partial x_j} + \dfrac{\partial {u_j}''^{(f)}}{\partial x_i}\right)$ is the strain rate of the fluctuating fluid velocity field and μ_f is the dynamic viscosity of the fluid–phase.

The first term on the right hand side of Eq. (20) represents the interphase transfer of kinetic energy denoted Π_{k_f} so that

$$\Pi_{k_f} = -\left\langle {u_i}''^{(f)} \tau_{ji} n_j^{(s)} \delta\left(\mathbf{x}-\mathbf{x}^{(I)}\right)\right\rangle, \tag{21}$$

which is non–zero at the fluid–solid interface owing to the Dirac delta function at $\mathbf{x}^{(I)}$. Ying and Subramaniam (2007) showed that for fixed particle assemblies the interphase kinetic energy transfer term simplifies to $\langle \mathbf{W} \rangle \cdot \left\langle \mathbf{S}_M^{(f)} \right\rangle$, where $\langle \mathbf{W} \rangle = \left\langle \mathbf{u}^{(f)} \right\rangle - \left\langle \mathbf{u}^{(s)} \right\rangle$ is the mean slip velocity between the solid and the fluid phases, and $\left\langle S_{Mi}^{(f)} \right\rangle = -\left\langle \tau_{ji} n_j^{(s)} \delta\left(\mathbf{x}-\mathbf{x}^{(I)}\right)\right\rangle$ is the average momentum transfer between the fluid and the solid phase. This simplification is possible because particles in a fixed bed are stationary and the fluid velocity field satisfies the no–slip condition at the particle surfaces, as a consequence of which $\mathbf{u}''^{(f)} = -\left\langle \mathbf{u}^{(f)} \right\rangle$ at every point on the fluid–particle interface in Eq. 21. For random assemblies, since the mean slip velocity is aligned with the mean interphase momentum transfer (Hill et al., 2001b; Tenneti et al., 2011), Π_{k_f} is positive and represents a source of gas–phase velocity fluctuations. The second term ($2\mu_f \langle I_f s_{ij} s_{ij} \rangle$) on the right hand side of Eq. (20)

is usually expressed as $\rho_f (1-\phi)\varepsilon_f$ where ε_f is the dissipation of k_f. Since $s_{ij}s_{ij}$ is always positive, ε_f represents a sink of k_f.

An expression for the interphase transfer of kinetic energy Π_{k_f} can be derived by expressing the interphase momentum transfer in terms of the average drag force acting per particle:

$$\Pi_{k_f} = \langle \mathbf{W} \rangle \cdot \left\langle \mathbf{S}_M^{(f)} \right\rangle = \frac{18\phi (1-\phi)^2 \mu_f}{D^2} F(\phi, \mathrm{Re}_m) |\langle \mathbf{W} \rangle|^2 . \tag{22}$$

In the above expression, $F(\phi, \mathrm{Re}_m)$ is the normalized average drag force per particle given by

$$F = \frac{|\langle \mathbf{F} \rangle|}{F_{\mathrm{Stokes}}}, \tag{23}$$

where $\langle \mathbf{F} \rangle$ is the average hydrodynamic force per particle and $F_{\mathrm{Stokes}} = 3\pi\mu_{\mathrm{f}} D (1-\phi) |\langle \mathbf{W} \rangle|$ is the Stokes drag acting on an isolated sphere moving with a slip velocity of $(1-\phi)|\langle \mathbf{W} \rangle|$. The expression for the source of k_f due to interface transfer of kinetic energy, derived in Eq. (22) is similar to the one derived by Crowe (2000). While Crowe (2000) used the single sphere drag correlation for $F(\phi, \mathrm{Re}_m)$, here we obtain this value directly from the particle–resolved DNS. An accurate correlation for $F(\phi, \mathrm{Re}_m)$ has been developed using the data obtained from PUReIBM simulations (Tenneti et al., 2011). The drag correlation is summarized below for the sake of completeness. The average normalized drag force acting per particle in flow past a random assembly of monodisperse spheres is given by

$$F(\phi, \mathrm{Re}_m) = \frac{F_{\mathrm{isol}}(\mathrm{Re}_m)}{(1-\phi)^3} + F_\phi(\phi) + F_{\phi,\mathrm{Re}_m}(\phi, \mathrm{Re}_m) \tag{24}$$

where, F_{isol} is the drag force acting on an isolated sphere moving in an unbounded medium. We used the drag correlation proposed by Schiller and

Nauman (1935) to get the drag on an isolated sphere. The remaining two terms in Eq. 24 are given by

$$\begin{aligned} F_{\phi}\left(\phi\right) &= \frac{5.81\phi}{\left(1-\phi\right)^{3}} + 0.48\frac{\phi^{1/3}}{\left(1-\phi\right)^{4}}, \\ F_{\phi,\mathrm{Re}_m}\left(\phi,\mathrm{Re}_m\right) &= \phi^{3}\mathrm{Re}_m\left(0.95 + \frac{0.61\phi^{3}}{\left(1-\phi\right)^{2}}\right). \end{aligned}$$

At steady state the source and sink of kinetic energy must balance each other i.e.,

$$\Pi_{k_f} = \rho_f\left(1-\phi\right)\varepsilon_f. \tag{25}$$

To our knowledge, all the turbulence models for multiphase flows use a Kolmogorov scaling for the dissipation term in a manner similar to single phase turbulence models i.e., $\varepsilon_f \sim k_f^{3/2}/l_K$. While in single–phase turbulence the length scale l_K in this expression corresponds to eddies in the inertial subrange, the corresponding interpretation in gas–solids flow is not clear. Note that the validity of the Kolmogorov scaling rests on the energy cascade hypothesis with a constant dissipation rate in the inertial subrange. These assumptions may not hold in gas–solids flow. An alternative expression for the dissipation rate in single–phase turbulence is $\varepsilon_f \sim 2\nu_f k_f/l_T^2$, where l_T is the Taylor microscale and ν_f is the kinematic viscosity of the fluid–phase. This expression can be generalized to any random velocity field with a finite spatial autocorrelation length. In the following we show that the Kolmogorov scaling does not yield a plausible behavior for l_K with Re_m for gas–solid flows with finite sized particles, whereas the behavior of l_T is reasonable.

Using the Kolmogorov scaling for the dissipation term and substituting

$\varepsilon_f = k_f^{3/2}/l_K$ in Eqs. (25) and (22) implies the following expression for l_K/D:

$$\frac{l_K}{D} = \left(\frac{k_f}{E_f}\right)^{3/2} \left(36\sqrt{2}\phi\left(1-\phi\right)^2 \frac{F\left(\phi, \mathrm{Re}_m\right)}{\mathrm{Re}_m}\right)^{-1}. \tag{26}$$

Similarly, using the Taylor microscale scaling for the dissipation term and substituting $\varepsilon_f = 2\nu_f k_f/l_T^2$ in Eqs. (25) and (22) results in the following expression for l_T/D:

$$\frac{l_T}{D} = \left(\frac{k_f}{E_f}\right)^{1/2} \left(18\phi\left(1-\phi\right) F\left(\phi, \mathrm{Re}_m\right)\right)^{-1/2}. \tag{27}$$

The behavior of the length scales l_K and l_T with solids volume fraction and mean flow Reynolds number can be inferred by substituting Eqs. (18) and (23) in Eqs. (26) and (27) respectively. The variation of l_K and l_T with solid volume fraction and Reynolds number are compared in Fig. 10. The behavior of length scale l_K obtained by modeling the dissipation term by Kolmogorov scaling ($\varepsilon_f \sim k_f^{3/2}/l_K$) is shown by dashed lines. This length scale increases with mean flow Reynolds number and decreases with volume fraction. The behavior of the length scale l_T obtained using a Taylor microscale scaling ($\varepsilon_f \sim 2\nu_f k_f/l_T^2$) is shown in Fig. 10 using solid lines. This length scale decreases with both mean flow Reynolds number and solids volume fraction.

For laminar flow past a single sphere, the length scale on which the velocity gradients vary is of the order of the boundary layer thickness δ/D which varies inversely with $\sqrt{\mathrm{Re}_m}$. We expect this length scale to decrease with increasing solids volume fraction. Since the hypothesis of energy cascade probably does not hold in homogeneous gas–solid flow with finite–sized particles, the applicability of the Kolmogorov scaling is questionable, as also evidenced by the behavior of l_K with Re_m. On the other hand, the scaling

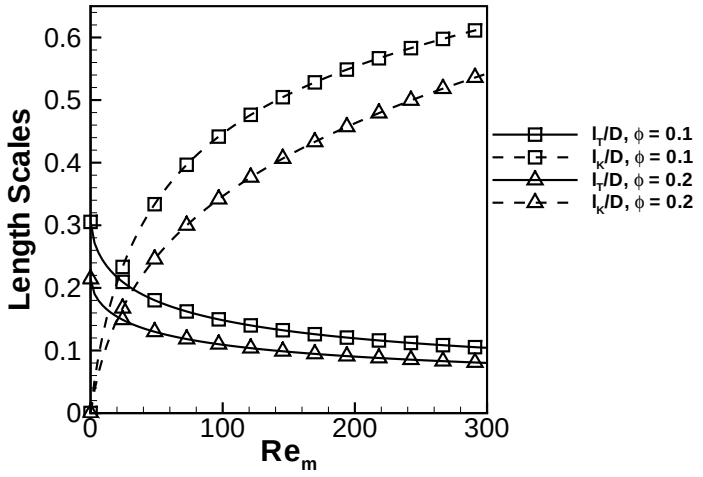

Figure 10: Variation of dissipation length scales with Reynolds number for solid volume fractions 0.1 and 0.2. Dashed lines are obtained by modeling the dissipation term as $k_f^{3/2}/l_K$ while the solid lines are obtained by modeling the dissipation as $2\nu_f k_f/l_T^2$.

of l_T indicates that the Taylor microscale is a better choice to model the dissipation term in gas–solid flows with finite sized particles. However, it must be noted that neither l_K nor l_T may correspond to the exact length scales of dissipative motions in gas–solids flow.

8. Eddy viscosity for gas–solid flow

In several studies the gas–phase Reynolds stress term is modeled in a fashion similar to single–phase turbulence i.e.,

$$\left\langle u_i''^{(f)} u_j''^{(f)} \right\rangle = \frac{2}{3}\delta_{ij}\left(k_f + \nu_t \frac{\partial \left\langle u_k^{(f)} \right\rangle}{\partial x_k}\right) - \nu_t \left(\frac{\partial \left\langle u_i^{(f)} \right\rangle}{\partial x_j} + \frac{\partial \left\langle u_j^{(f)} \right\rangle}{\partial x_i}\right).$$

In this model ν_t is the eddy viscosity for gas–solid flow and it depends on the turbulent kinetic energy (k_f) and dissipation rate (ε_f) through the relation

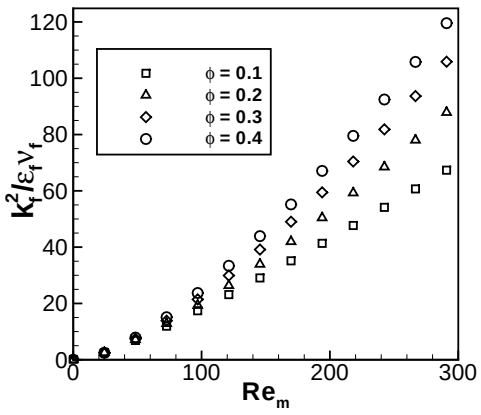

Figure 11: Behavior of the ratio $k_f^2/(\varepsilon_f \nu_f)$ with mean flow Reynolds number for different solid volume fractions.

$\nu_t = C_\mu k_f^2/\varepsilon_f$. In this relation C_μ is a model constant and usually the value for the constant associated with the $k-\varepsilon$ models of single–phase turbulence are used in gas–solid flows as well. Since we have quantified both k_f (cf. Eq. (18)) and ε_f (cf. Eq. (25)) using particle–resolved DNS, we can infer an eddy viscosity for gas–solid flow as a function of solid volume fraction and mean flow Reynolds number. The ratio $k_f^2/(\varepsilon_f \nu_f)$ is shown as a function of Re_m for different ϕ in Fig. 11. We see that the ratio $k_f^2/(\varepsilon_f \nu_f)$ increases with both solid volume fraction and mean flow Reynolds number. This dependence on the mean flow Reynolds number indicates that the transport of gas–phase Reynolds stress can become important if there are large gradients in the mean flow and solid volume fraction, as found in many multiphase flow applications. Further, the PR–DNS of Mehrabadi et al. (2012) shows that the value of k_f in freely evolving gas–solid suspensions is very close to that observed in fixed–beds. This observation confirms the applicability of the

proposed eddy viscosity model in device–scale CFD simulations of gas–solid flow applications.

9. Conclusions

In this work we quantified the strength of gas–phase velocity fluctuations in gas–solid flows as a function of solids volume fraction and Reynolds number based on mean slip velocity using PR–DNS of steady flow past fixed particle assemblies. We employ the Particle–resolved Uncontaminated–fluid Reconcilable Immersed Boundary Method (PUReIBM) to perform PR–DNS of flow past fixed particle assemblies. We observe that the presence of particles generates high level of fluctuations in the gas velocity. The kinetic energy in the fluctuating motions (k_f) can be as high as the kinetic energy in the mean motion (E_f), especially for systems with higher solid volume fraction greater than 0.4. The ratio k_f/E_f increases with the solids volume fraction and decreases with mean flow Reynolds number. We observe that the gas–phase Reynolds stress in the bed is anisotropic at all Reynolds numbers and volume fractions. Based on the PUReIBM PR–DNS data, we propose a correlation for k_f/E_f in terms of solid volume fraction and mean flow Reynolds number. Our results indicate that the use of a length scale analogous to Taylor microscale is appropriate to model the dissipation term in gas–solid flows. Using the PUReIBM PR–DNS data for k_f and ε_f we infer an eddy viscosity that can be used in predictive CFD simulations of gas-solid flow.

Appendix A. Simplification of the covariance of fluctuating velocity and gradient of stress tensor to dissipation in statistically homogeneous gas–solid flow

As discussed in section 7, the conservation equation for k_f in statistically homogeneous flows is written as

$$\frac{\partial}{\partial t}\{(1-\phi)\,\rho_f k_f\} = -\left\langle {u_i}''^{(f)} \tau_{ji} n_j^{(s)} \delta\left(\mathbf{x}-\mathbf{x}^{(I)}\right)\right\rangle + \left\langle {u_i}''^{(f)} \frac{\partial\left(I_f \tau_{ji}\right)}{\partial x_j}\right\rangle. \tag{A.1}$$

In this equation τ_{ji} is the fluid phase stress tensor given by

$$\tau_{ji} = -p\delta_{ji} + \mu_f\left(\frac{\partial u_i}{\partial x_j} + \frac{\partial u_j}{\partial x_i}\right),$$

where p and $\mathbf{u}$ are the instantaneous pressure and velocity fields respectively. The second term on the right hand side is the covariance of the fluctuating fluid velocity field and the gradient of the stress tensor in the fluid phase. Using the product rule this term can be written as

$$\left\langle {u_i}''^{(f)} \frac{\partial\left(I_f \tau_{ji}\right)}{\partial x_j}\right\rangle = \left\langle \frac{\partial}{\partial x_j}\left(I_f {u_i}''^{(f)} \tau_{ji}\right)\right\rangle - \left\langle I_f \tau_{ji} \frac{\partial {u_i}''^{(f)}}{\partial x_j}\right\rangle. \tag{A.2}$$

Commuting the gradient and averaging operators and invoking the assumption of statistical homogeneity, the first term on the right hand side of the above equation simplifies to zero. The second term on the right hand side can be further simplified by considering the definition of the stress tensor:

$$\tau_{ji}\frac{\partial {u_i}''^{(f)}}{\partial x_j} = \left(-p\delta_{ji} + \mu_f\left(\frac{\partial {u_i}''^{(f)}}{\partial x_j} + \frac{\partial {u_i}''^{(f)}}{\partial x_j}\right)\right)\frac{\partial {u_j}''^{(f)}}{\partial x_i} \tag{A.3}$$

Since the fluctuating velocity field is divergence free, the pressure term is zero. So the above equation reduces to:

$$\tau_{ji}\frac{\partial {u_i}''^{(f)}}{\partial x_j} = \mu_f\left[\frac{\partial {u_i}''^{(f)}}{\partial x_j}\frac{\partial {u_i}''^{(f)}}{\partial x_j} + \frac{\partial^2}{\partial x_i \partial x_j}\left({u_i}''^{(f)} {u_j}''^{(f)}\right)\right] = 2\mu_f s_{ij} s_{ij}, \tag{A.4}$$

where, $s_{ij} = \frac{1}{2}\left(\frac{\partial {u_i}''^{(f)}}{\partial x_j} + \frac{\partial {u_j}''^{(f)}}{\partial x_i}\right)$. Therefore, the second term on the right hand side of Eqs. (A.1) and (19) simplifies to

$$\left\langle {u_i}''^{(f)} \frac{\partial \left(I_f \tau_{ji}\right)}{\partial x_j} \right\rangle = -2\mu_f \left\langle I_f s_{ij} s_{ij} \right\rangle , \tag{A.5}$$

which is strictly negative and can be identified as the dissipation rate of k_f in statistically homogeneous gas–solid flow.

Acknowledgments

This work is partially supported by Department of Energy grant DE–FC26–07NT43098 through the National Energy Technology Laboratory (NETL). We would like to acknowledge the National Science Foundation for partial support from award CBET 1134500. We would also like to acknowledge Professor Rodney Fox for the suggestion to calculate the implied eddy viscosity for gas–solid flow.

References

Agrawal, K., Loezos, P., Syamlal, M., Sundaresan, S., October 2001. The role of meso-scale structures in rapid gas-solid flows. J. Fluid Mech. 445, 151–181.

Ahmadi, G., Ma, D., 1990a. A thermodynamical formulation for dispersed multiphase turbulent flows: II simple shear flows for dense mixtures. Intl. J. Multiphase Flow 16 (2), 341–351.

Ahmadi, G., Ma, D., 1990b. A thermodynamical formulation for dispersed multiphase turbulent flows: I basic theory. Intl. J. Multiphase Flow 16 (2), 323–340.

Anderson, T. B., Jackson, R., 1967. A fluid mechanical description of fluidized beds. Ind. Eng. Chem. Fundam. 6, 527–539.

Bagchi, P., Balachandar, S., 2003. Effect of turbulence on the drag and lift of a particle. Phys. Fluids 15 (11), 3496–3513.

Balachandar, S., Eaton, J. K., 2010. Turbulent dispersed multiphase flow. Annu. Rev. Fluid Mech. 42, 111–133.

Balzer, G., Boelle, A., Simonin, O., 1998. Eulerian gas–solid flow modelling of dense fluidized bed. In: Fluidization VIII. International Symposium of Engineering Foundation, pp. 1125–1134.

Beetstra, R., van der Hoef, M. A., Kuipers, J. A. M., 2007. Drag force of intermediate Reynolds number flows past mono– and bidisperse arrays of spheres. A.I.Ch.E.J. 53, 489.

Benyahia, S., Syamlal, M., O'Brien, T. J., 2005. Evaluation of boundary conditions used to model dilute, turbulent gas/solids flows in a pipe. Powder Technology 156, 62–72.

Boivin, M., Simonin, O., Squires, K. D., 1998. Direct numerical simulation of turbulence modulation by particles in isotropic turbulence. J. Fluid Mech. 375, 235–263.

Bolio, E., Sinclair, J., 1995. Gas turbulence modulation in the pneumatic conveying of massive particles in vertical tubes. Intl. J. Multiphase Flow 21 (6), 985–1001.

Bolio, E., Yasuna, J., Sinclair, J., 1995. Dilute turbulent gas-solid flow in risers with particle-particle interactions. A.I.Ch.E.J. 41 (5), 1375 – 1388.

Burton, T. M., Eaton, J. K., 2005. Fully resolved simulations of particle–turbulence interaction. J. Fluid Mech. 545, 67–111.

Clift, R., Grace, J. R., Weber, M. E., 1978. Bubbles, Drops and Particles. Academic Press.

Cocco, R., Shaffer, F., Hays, R., Reddy Karri, S. B., Knowlton, T., 2010. Particle clusters in and above fluidized beds. Powder Technology 203 (1), 3–11.

Cornish, R. J., 1928. Flow in a pipe of rectangular cross-section. Proceedings of the Royal Society of London. Series A, Containing Papers of a Mathematical and Physical Character 120 (786), 691–700.

Crowe, C. T., 2000. On models for turbulence modulation in fluid–particle flows. Intl. J. Multiphase Flow 26, 719–727.

Crowe, C. T., Troutt, T. R., Chung, J. N., 1996. Numerical models for two–phase turbulent flows. Annu. Rev. Fluid Mech. 28, 11–43.

Cundall, P. A., Strack, O. D. L., 1979. A discrete numerical model for granular assemblies. Geotechnique 29, 47–65.

Drew, D. A., 1983. Mathematical modeling of two–phase flow. Annu. Rev. Fluid Mech. 15, 261–291.

Drew, D. A., Passman, S. L., 1998. Theory of Multicomponent Fluids. Applied Mathematical Sciences. Springer, New York.

Elghobashi, S. E., Truesdell, G. C., 1993. On the two-way interaction between homogeneous turbulence and dispersed solid particles. I: Turbulence modification. Phys. Fluids A 5, 1790–1801.

Ergun, S., 1952. Fluid flow through packed columns. Chem. Eng. Prog. 48, 89–94.

Garg, R., 2009. Modeling and simulation of two-phase flows. Ph.D. thesis, Iowa State University.

Garg, R., Galvin, J., Li, T., Pannala, S., 2010a. Documentation of open–source MFIX–DEM software for gas–solids flows. Tech. rep., National Energy Technology Laboratory, Department of Energy.
URL `https://www.mfix.org`

Garg, R., Tenneti, S., Mohd-Yusof, J., Subramaniam, S., 2010b. Direct numerical simulation of gas-solids flow based on the immersed boundary method. In: Pannala, S., Syamlal, M., O'Brien, T. J. (Eds.), Computational Gas-Solids Flows and Reacting Systems: Theory, Methods and Practice. IGI Global.

Gidaspow, D., 1994. Multiphase Flow and Fluidization. Academic Press.

Halvorsen, B., Guenther, C., O'Brien, T. J., 2003. CFD calculations for scaling of a bubbling fluidized bed . In: Proceedings of the AIChE annual meeting. AIChE, San Francisco, CA, pp. 16–21.

Hill, R. J., Koch, D. L., Ladd, A. J. C., 2001a. The first effects of fluid inertia on flows in ordered and random arrays of spheres. J. Fluid Mech. 448 (213-241).

Hill, R. J., Koch, D. L., Ladd, A. J. C., 2001b. Moderate–Reynolds–number flows in ordered and random arrays of spheres. J. Fluid Mech. 448 (243-278).

Hrenya, C. M., Sinclair, J. L., 1997. Effects of particle-phase turbulence in gas-solid flows. AIChE Journal 43 (4), 853–869.

Kashiwa, B., Gaffney, E., 2003. Design Basis for CFDLib. Tech. Rep. LA-UR-03-1295, Los Alamos National Lab.

Kenning, V. M., Crowe, C. T., 1997. On the effect of particles on carrier phase turbulence modulation in gas–particle flows. Intl. J. Multiphase Flow 23 (2), 403–408.

Kim, J., Moin, P., 1985. Application of a fractional-step method to incompressible Navier-Stokes equations. Journal of Computational Physics 59, 308–323.

Lucci, F., Ferrante, A., Elghobashi, S., 2011. Is Stokes number an appropriate indicator for turbulence modulation by particles of Taylor–length–scale size? Phys. Fluids 23 (2), 025101–025101–7.

Lumley, J. L., Newman, G. R., 1977. The return to isotropy of homogeneous turbulence. J. Fluid Mech. 82, 161–178.

Mashayek, F., Taulbee, D. B., 2002. Turbulent gas–solid flows, part I: Direct numerical simulations and Reynolds stress closures. Numerical Heat Transfer, Part B: Fundamentals 41 (1), 1–29.

Mehrabadi, M., Tenneti, S., Subramaniam, S., 2012. Gas–phase velocity fluctuations in statistically homogeneous fixed particle beds and freely evolving suspensions using particle–resolved direct numerical simulation, in review.

Miller, A., Gidaspow, D., 1992. Dense, vertical gas–solid flow in a pipe. A.I.Ch.E.J. 38 (11), 1801–1815.

Modarress, D., Tan, H., Elghobashi, S. E., 1984. Two–component LDA measurement in a two–phase turbulent jet. AIAA Journal 22, 624–630.

Moran, J. C., Glicksman, L. R., 2003. Mean and fluctuating gas phase velocities inside a circulating fluidized bed. Chemical Engineering Science 58, 1867–1878.

Pai, M. G., Subramaniam, S., 2009. A comprehensive probability density function formalism for multiphase flows. Journal of Fluid Mechanics, 181–228.

Patankar, S. V., 1980. Numerical heat transfer and fluid flow. Hemisphere Pub. Corp. ; McGraw-Hill.

Pope, S. B., 2000. Turbulent Flows. Cambridge University Press, Port Chester, NY.

Schiller, L., Nauman, A., 1935. A drag coefficient correlation. V.D.I. Zeitung.

Squires, K. D., Eaton, J. K., 1991. Measurements of particle dispersion obtained from direct numerical simulations of isotropic turbulence. J. Fluid Mech. 226, 1–35.

Subramaniam, S., 2000. Statistical representation of a spray as a point process. Phys. Fluids 12 (10), 2413–2431.

Sun, J., Battaglia, F., Subramaniam, S., November 2007. Hybrid Two-Fluid DEM Simulation of Gas-Solid Fluidized Beds. Journal of Fluids Engineering 129 (11), 1394–1403.

Sundaram, S., Collins, L. R., 1999. A numerical study of the modulation of isotropic turbulence by suspended particles. J. Fluid Mech. 379, 105–143.

Syamlal, M., Rogers, W., O'Brien, T. J., 1993. MFIX Documentation: Theory Guide. Tech. Rep. DOE/METC-95/1013, NTIS/DE95000031, National Energy Technology Laboratory, Department of Energy, see also URL http://www.mfix.org.

Syamlal, M. and O'Brien, T. J., 1987. A generalized drag correlation for multiparticle systems. Tech. rep., Morgantown Energy Technology Center DOE Report.

Tenneti, S., Garg, R., Hrenya, C. M., Fox, R. O., Subramaniam, S., 2010. Direct numerical simulation of gas–solid suspensions at moderate Reynolds number: Quantifying the coupling between hydrodynamic forces and particle velocity fluctuations. Powder Technology 203 (1), 57–69.

Tenneti, S., Garg, R., Subramaniam, S., 2011. Drag law for monodisperse gas–solid systems using particle–resolved direct numerical simulation of flow past fixed assemblies of spheres. Intl. J. Multiphase Flow 37 (9), 1072–1092.

Tsuji, Y., Morikawa, Y., Shiomi, H., 1984. LDV measurements of an air–solid two–phase flow in a vertical pipe. J. Fluid Mech. 139, 417–434.

Uhlmann, M., 2008. Interface–resolved direct numerical simulation of vertical particulate channel flow in the turbulent regime. Phys. Fluids 20 (5), 053305–053305–27.

van der Hoef, M. A., Beetstra, R., Kuipers, J. A. M., 2005. Lattice-Boltzmann simulations of low-Reynolds-number flow past mono- and bidisperse arrays of sphere: Results for the permeability and drag force. J. Fluid Mech. 528, 233–254.

Wang, Q., Squires, K. D., Simonin, O., 1998. Large eddy simulation of turbulent gas–solid flows in a vertical channel and evaluation of second–order models. Intl. J. Heat and Fluid Flow 19, 505–511.

Wen, C. Y., Yu, Y. H., 1966. Mechanics of fluidization. Chem. Eng. Prog. Symp. Series 62, 100–111.

Xu, Y., Subramaniam, S., 2010. Effect of particle clusters on carrier flow turbulence: A direct numerical simulation study. Flow, Turbulence and Combustion 85, 735–761, 10.1007/s10494-010-9298-8.
URL http://dx.doi.org/10.1007/s10494-010-9298-8

Yarin, L., Hetsroni, G., 1994. Turbulence intensity in dilute two-phase flows–1: Effect of particle-size distribution on the turbulence of the carrier fluid. International Journal of Multiphase Flow 20 (1), 1–15.

Ying, X., Subramaniam, S., 2007. Consistent modeling of interphase turbulent kinetic energy transfer in particle-laden turbulent flows. Physics of Fluids 19 (8), 085101.

Yuan, Z., Michaelides, E. E., 1992. Turbulence modulation in particulate flows–a theoretical approach. International Journal of Multiphase Flow 18 (5), 779–785.

Yusof, J. M., 1996. Interaction of massive particles with turbulence. Ph.D. thesis, Cornell University.

Zhang, Y. H., Reese, J. M., 2003. Gas turbulence modulation in a two–fluid model for gas–solid flows. A.I.Ch.E.J. 49 (12), 3048–3065.

Zick, A. A., Homsy, G. M., 1982. Stokes flow through periodic arrays of spheres. J. Fluid Mech. 115, 13–26.